Structural Eng. / Earthquake Eng. Vol. 5. No. 1, 21s-29s. April 1988
Japan Society of Civil Engineers (Proc. of JSCE No. 392/I-9)

AN EXPERIMENTAL STUDY ON STRENGTH OF THIN-WALLED STEEL BOX BEAM-COLUMNS UNDER REPETITIVE BENDING

By Eiichi WATANABE, Susumu EMI**, Hidenori ISAMI*** and Tohru YAMANOUCHI*****

This study presents an experimental investigation on the strength of thin-walled steel box beam-columns of the T-shaped steel bridge piers under constant axial thrust and repetitive bending moment simulating earthquake excitations being applied, however, in the static condition. The steel box beam-column specimens had flanges with or without the longitudinal stiffeners.

From the tests, the elasto-plastic behavior, the ultimate strength, the deteriorating and hysteretic properties are clarified. The effects such as the rigidity of the flange stiffeners, the magnitude of the axial force on the load-carrying capacity and the failure types of the specimens are investigated.

Keywords : steel bridge piers, box beam-columns, repetitive bending

1. INTRODUCTION

In Japan, most of the urban elevated highway systems are constructed on soft sedimented basin. These elevated highways, especially the foundation and the structural components near the intersections of the superstructure and the substructure are considered to be quite vulnerable to the earthquake excitations. In fact, a great number of earthquake damages have been reported so far on R. C. bridge piers.

In view of the fact that a great number of steel piers have been constructed in our big cities such as Tokyo Metropolis and Osaka, it seems to be of great importance to investigate their aseismatic strength and the safety. Fortunately, our big cities have scarcely experienced earthquakes of big magnitude in these years ; consequently, no significant damages have been reported on steel bridge piers. Thus, there is a definite need to investigate by experimental means the aseismic resistance of the steel bridge piers. Specifically, the mode of failure, the maximum earthquake acceleration that the piers can withstand, aseismic diagnosis of the existing piers, and the establishment of the reasonable procedure of the aseismic design are among the most important subjects of our concern.

In general, structures must meet two basic criteria of seismic design : large stiffness at working load and large ductility and dissipating large amount of energy at overloads[1)~7)]. However, this may be hindered by brittle type of failure including bucklings. In fact, the steel bridge piers usually consist of thin-walled stiffened plates and thus are essentially liable to bucklings.

A great number of researches have been conducted on the static strengths of compressed steel stiffened

* Member of JSCE, Ph. D. & Dr. Eng., Professor, Kyoto University (Yoshida-Honmachi, Sakyoku, Kyoto 606)
** Member of JSCE, Hanshin Express Highway Authority (4-68, Kita-Kyutaroh-chou, Higashi-ku, Osaka 541)
*** Member of JSCE, Dr. Eng., Associate Professor, Kohchi National College of Technology (200-1, Monobe-Otsu, Nangoku, Kohchi 783)
**** Member of JSCE, M. S., Engineer, Osaka Gas Company (5-1, Hirano-cho, Higashi-ku, Osaka 541)

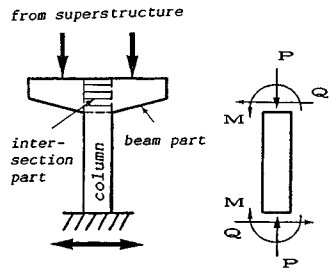

Fig. 1 Modelling of T-shaped Steel Bridge Piers.

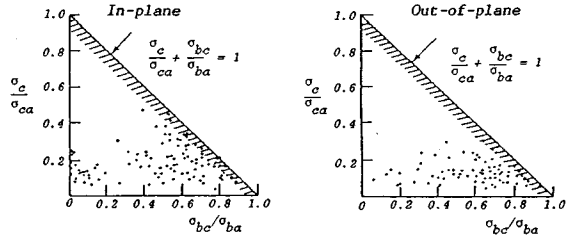

Fig. 2 Interaction of the Axial Compressive Stress and the Compressive Bending Stress of Steel Bridge Piers.

plates and box girders. However, the studies pertaining to the cyclic loading are still insufficient[8], and there is definitely a great need for them. This study is concerned with the box column of the T-shaped steel bridge piers such as shown in Fig. 1. This portion is identified as a beam-column subjected to a constant axial force, P, and a statically applied but slowly varying bending moment, M, simulating a basic part of dynamically varying earthquake motions[9].

2. DESCRIPTION OF TESTS

(1) Test specimens

According to the 1973 JSHB[10], the axial compressive stress, σ_c, and the compressive bending stress, σ_{bc}, must satisfy the following inequality :

$$\frac{\sigma_c}{\sigma_{ca}}+\frac{\sigma_{bc}}{\sigma_{ba}}<1 \quad \cdots\cdots (1)$$

where σ_{ca} and σ_{ba} refer to the allowable axial compressive stress and the allowable compressive bending stress, respectively. Nakai et al.[11] have surveyed this inequality for 88 steel rigid frame bridge piers in Osaka area that have been already constructed according to the 1973 codes of JSHB[10]. Fig. 2 illustrates their results. From this, the following observations may be made :

(i) The values of σ_c/σ_{ca} scatter about 0.2 with the maximum of 0.6 in case of the in-plane bending, and 0.3 in case of the out-of-plane bending of the bridge piers.

(ii) The values of σ_{bc}/σ_{ba} scatter continuously between 0 and 1.0 and the most frequently between 0.4 and 0.9, showing the earthquake loads can be frequently decisive.

Taking these in mind, the test specimens are designed as the beam-columns that are subjected to the loading of either (i) without the axial thrust or (ii) with the axial thrust of $P/P_Y=0.2$, as shown in Fig. 3, where P_Y designates the squash load.

Although there seem to be several differences in stress-strain relationships between the dynamic and static responses[6),12),13)], and the effect of the inertia forces seems to be important as well, it is assumed to be negligible since no significant differences of results were reported to be observed[9] after the comparison of dynamic test of 1 Hz and the static tests. Thus, the tests are performed herein in such a way that the constant axial load is generated by the horizontal actuator ; whereas, the bending moment is generated statically by the vertical actuator in the stroke control mode simulating the basic portion of a big earthquake excitation[1),4),9),13)].

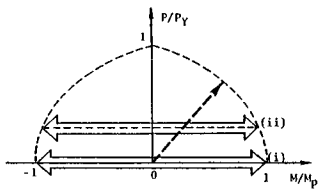

Fig. 3 Loading Types.
(i) without Axial Thrust.
(ii) with Axial Thrust. $P/P_Y=0.2$.

Fig. 4 illustrates the box test specimens. These specimens form a part of the longer beam-column as shown in the whole view of the system of Fig. 5 under pure bending with or without axial thrust. The test specimens are fastened by high-tension bolts to the end beams which are designed as non-destructive components and thus for repeated use.

The test specimens are classified into three types of A, B and C,

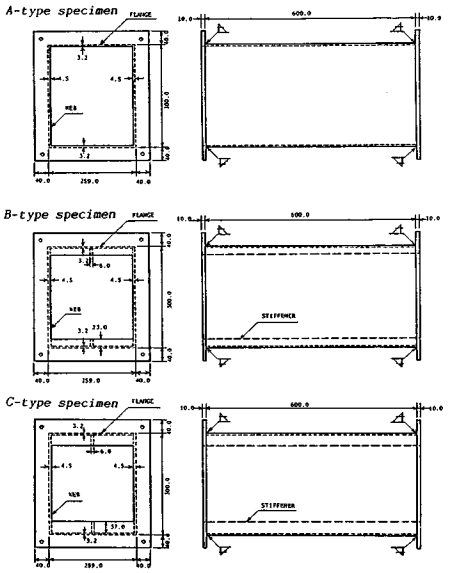

Fig. 4 Test Specimens. A, B and C.

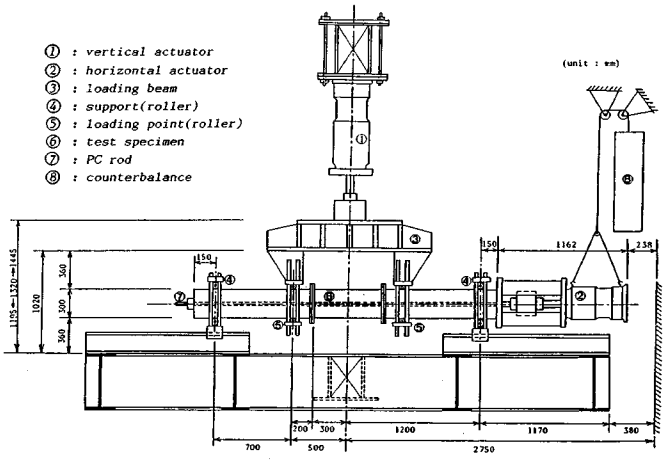

Fig. 5 Test Setup. Bi-Axial Testing System.

depending on the longitudinal stiffeners. They correspond to the unstiffened flanges, stiffened flanges with $\gamma/\gamma^*=1$ and $\gamma/\gamma^*=3$, respectively, where

$$\gamma \equiv \frac{EI}{bD} \quad \text{and} \quad \gamma^* = \frac{\alpha^2}{n}\{4n^2(1+n\delta)-2\} - \frac{\alpha^4}{n} + \frac{1+n\delta}{n} \qquad (2)$$

where E, I and $D=Et^3/[12(1-\nu^2)]$ refer to Young's modulus, moment of inertia of a longitudinal stiffener and flexural rigidity of isotropic plate, respectively. Also, ν, t, a and b refer to the Poisson's ratio, thickness, length and width of the plate, respectively; $\alpha=a/b$, n and $\delta=A_s/(bt)$ refer to aspect ratio of plate, number of plate panels as divided by the stiffeners, and ratio of the cross-sectional area of a stiffener, respectively. Furthermore, γ^* designates the minimum required rigidity given according to the DIN 4114[16),17)], but it is very close to that specified by the JSHB[18)].

Tables 1, 2 and 3 list the actual dimensions, various predicted strengths on the basis of the results of the material tests, and the cross-sectional parameters, respectively, where in Table 2, P_u is predicted by the approximate equation : $P_u=2W\sigma_u/c$, where W, c and σ_u refer to the elastic section modulus of the specimen, horizontal distance between the position of the load and a roller support, and compressive strength of the flange plate, respectively. In these tables, the first subscript "2" of the specimen A_{21}, for example, designates the application of axial thrust as compared with the script "1" indicating the absence

Table 1 Actual Dimensions of Test Specimens (in mm).

Test Specimen	Flange 1		Flange 2		Web 1		Web 2		Stiffener 1		Stiffener 2		Length
	B_1	t_{f1}	B_2	t_{f2}	D_1	t_{w1}	D_2	t_{w2}	h_1	t_{s1}	h_2	t_{s2}	L
A11	257.9	3.05	257.9	3.06	299.8	4.35	300.0	4.36	—	—	—	—	599.6
A12	257.9	3.10	257.8	3.05	299.6	4.47	299.9	4.36	—	—	—	—	599.6
A21	258.2	3.06	258.0	2.99	299.6	4.43	299.9	4.33	—	—	—	—	599.9
A22	258.0	3.04	257.9	3.04	300.0	4.44	299.5	4.48	—	—	—	—	599.9
B11	258.1	3.15	258.3	3.12	299.5	4.44	299.6	4.44	23.3	5.92	23.4	5.97	599.5
B12	258.1	3.22	258.0	3.35	299.4	4.46	299.7	4.43	22.7	5.98	22.6	5.99	599.8
B21	258.6	3.20	258.2	3.18	299.8	4.43	300.1	4.48	23.0	5.91	23.2	6.01	599.9
B22	258.3	3.28	258.0	3.32	299.8	4.32	299.9	4.33	22.9	6.00	23.0	6.01	599.6
C11	257.9	3.14	258.0	3.14	299.7	4.41	299.5	4.44	37.5	5.81	37.7	5.83	599.8
C12	257.9	3.14	257.6	3.14	299.8	4.41	299.7	4.38	36.1	5.86	37.3	5.78	599.6
C21	258.0	3.14	258.0	3.14	299.9	4.34	299.6	4.46	37.0	5.80	36.9	5.77	599.6
C22	258.0	3.14	257.9	3.14	299.7	4.44	299.8	4.43	37.9	5.82	37.8	5.81	599.8

Table 2 Predicted Strengths of Test Specimens (in tf).

Specimen	P_u	P_y	P_p	P_{sq}
A11	14.9	24.3	29.0	99.4
A12	15.1	24.5	29.2	100.4
A21	14.7	24.2	28.9	99.3
A22	14.9	24.4	29.2	100.5
B11	26.2	27.2	32.2	108.1
B12	27.0	27.9	32.9	109.9
B21	26.6	27.5	32.5	109.0
B22	27.1	27.8	32.7	108.5
C11	28.1	28.1	33.4	111.8
C12	28.0	28.0	33.2	111.1
C21	28.0	28.0	33.2	111.2
C22	28.2	28.2	33.5	112.0

Table 3 Cross-Sectional Parameters of Test Specimens.

Specimen	Area A(cm²)	Inertia Moment I_y(cm⁴)	Aspect Ratio α		Width-Thickness Ratio R			δ	γ/γ*
			Flange	Web	Flange	Web	Stiffnr.		
A11	41.35	5319.5	2.406	2.041	1.483	1.191	—	—	—
A12	41.78	5362.0	2.408	2.042	1.472	1.174	—	—	—
A21	41.34	5294.1	2.406	2.043	1.498	1.185	—	—	—
A22	41.88	5337.2	2.409	2.043	1.491	1.164	—	—	—
B11	45.01	5938.8	2.405	2.044	0.723	1.168	0.255	0.178	1.075
B12	45.71	6091.8	2.407	2.047	0.689	1.165	0.246	0.166	0.896
B21	45.40	6017.6	2.404	2.043	0.712	1.164	0.251	0.172	1.004
B22	45.16	6075.1	2.403	2.043	0.688	1.199	0.248	0.168	0.921
C11	46.53	6144.1	2.408	2.045	0.722	1.171	0.419	0.280	3.289
C12	46.25	6125.8	2.408	2.043	0.721	1.179	0.409	0.273	3.106
C21	46.30	6129.1	2.406	2.043	0.722	1.179	0.414	0.274	3.161
C22	46.63	6162.1	2.408	2.044	0.722	1.169	0.422	0.282	3.352

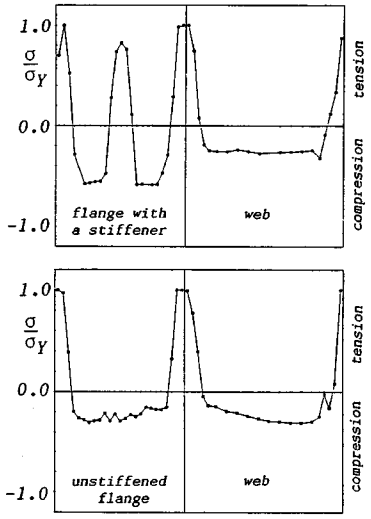

Fig. 6 Measured Residual Stress Distributions.

of the axial thrust ; and the second subscript "1" designates only the numbering.

(2) Material tests and residual stresses

A series of JIS standard tests were conducted using No. 5 standard specimens to find the yielding strength, the Young's modulus and the Poisson's ratio for each of the thicknesses of 3. 2 mm, 4. 5 mm and 6. 0 mm. Each specimen was found to behave perfectly elasto-plastically with the vertical yielding plateau, and the mean yielding strength was found to be about 2 500, 2 260 and 3 370 kg/cm² (250, 226 and 337 MPa), respectively for t=3. 2, 4. 5 and 6. 0 mm.

The residual stresses were measured for a specimen with unstiffened flanges and for another specimen with stiffened flanges, using strain gauges by means of the stress relieving and cutting out small strips from the vicinity of the center line of the specimens. The results of the measurement are illustrated for an unfolded flange and a web as shown in Figs. 6 . It may be obvious that the maximum magnitude of the tensile residual stress almost reaches the yielding stress along the intersection of the web with the flanges or along the joint of the stiffener with the flange plate, and the maximum magnitude of the compressive residual stress is distributed uniformly at 0. 2~0. 3 σ_Y in the web plate and the unstiffened flange or at about 0. 6 σ_Y on the plate panels of stiffened flange, respectively.

(3) Displacement transducers and strains

The measurement of the initial imperfections of the out-of-plane deflections and the residual deflections of the surfaces of the test specimens are considered to be of great importance, thus a special device was invented in such a way that totally 15 displacement transducers are fixed to a channel-shaped motor-driven rigid frame moving back and forth in the axial direction along and outside of the test specimen for the measurement of the out-of-plane deflections. Then, 15 out-of-plane deflections are measured for each of totally 11 cross sections.

Two displacement transducers to measure the global curvature of the test specimens and the vertical displacements are also installed herein. Let Φ, u_1 and u_2 designate the curvature, the reading of the upper displacement transducer for the curvature and that of the lower transducer, respectively, then the curvature, Φ, can be obtained by : $\Phi=(u_1-u_2)/(Ld_t)$, where L and d_t refer to the length of the specimen and the vertical distance between two transducers, respectively.

The strains are measured only at the cross section of the central part of the specimen. The interval of the gauges are determined to keep away from the track of the displacement transducers just mentioned above and for economical reasons.

(4) Testing and loading procedures

The servo-controlled testing system is utilized using two microcomputers[14),15)].

The loading is determined to be applied in the stroke control mode in a sequence of ramp wave forms as shown in Fig. 7 following the one adopted in references[9),13)].

3. RESULTS OF LOADING TESTS

(1) Strength interaction curves and moment-curvature relationships

Figs. 8 to 10 present some of the interactions between the peak bending moment and the axial load, in which each point corresponds to each loading cycle, for three different types of the specimens, plotted against three interaction curves of the JRA Specifications, the elastic limit line and the fully plastic curve. Herein, the positive or negative loading refers to the sagging or hogging, respectively.

From these figures, the following characteristics are observed for each type of specimens :

A-type The peak bending moments in each cycle are shown to occur within the linear elastic limit line, and, in general, their magnitudes decrease gradually after reaching the maximum bending moment as the loading cycles are increased. This is mainly caused by the elastic buckling of compressed flange plates. The peak bending moments in the last loading cycle are found to be 0.37~0.58 or 0.67~0.75 of the maximum bending moments in case of with or without the axial thrust, respectively. The axial thrust will be seen to reduce the maximum strength by about 18%.

B-type The peak bending moments in each loading cycle are shown to occur in the elasto-plastic range. The peak bending moments in the last loading cycle are found to be 0.61~0.87 or 0.90~0.93 of the maximum bending moments in case of with or without the axial thrust, respectively. In this case, the axial thrust will be seen to reduce the maximum strength by about 10%.

C-type The peak bending moments in each cycle are shown to occur in the elasto-plastic range and sometimes exceed the fully plastic curve. Then, the compressed flange plates of the specimens do not buckle and thus, remain stable in the elasto-plastic range. The peak bending moments develop in the fully plastic state. The peak bending moments in the last loading cycle are found to be 0.61~0.66 or about 0.93 of the maximum bending moments in case of with or without the axial thrust, respectively. In view of the

specimen	d_0 (mm)	Δ	specimen	d_0 (mm)	Δ
A11	4.0	0.5	A21	4.0	0.375
A12	4.0	0.375	A22	3.0	0.1875
B11	4.0	0.375	B21	3.0	0.1875
B12	4.0	0.375	B22	3.0	0.1875
C11	4.0	0.375	C21	3.0	0.1875
C12	4.0	0.375	C22	3.0	0.1875

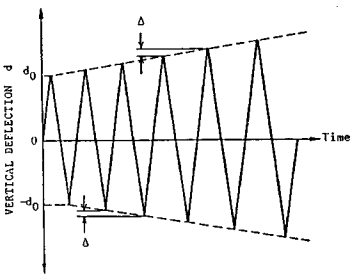

$$d_n = [\,1 + (n-1)\Delta\,]\, d_o$$

where
d_n : the maximum vertical deflection in the n-th loading cycle
d_o : the prescribed deflection in the first loading cycle
Δ : the ratio of the amplitude in the previous cycle to that in the present cycle, usually specified from the preliminary tests

Fig. 7 Sequential Ramp Wave Forms for Loading Criterion.

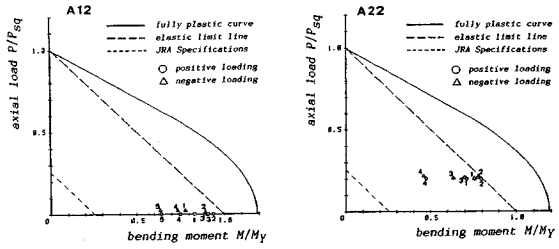

Fig. 8 Interaction Curves of Axial Thrust and Bending Moment. A-types.

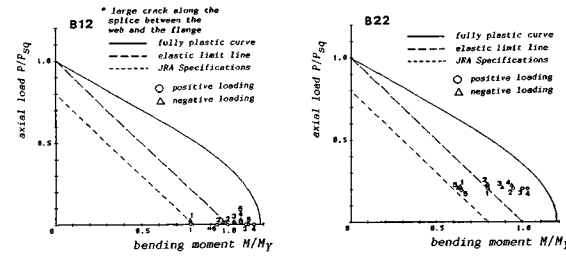

Fig. 9 Interaction Curves of Axial Thrust and Bending Moment. B-types.

fact that the number of repetitive cycles of the C-type specimens are larger than that of the B-type specimens, it looks as though that the peak maximum bending moments in case of C-type are more reduced than that in case of B-type. However, if the number of cycles is kept constant, it may be seen that the axial thrust will reduce the maximum strength by only about 2%. Therefore, it is seen that the C-type specimens are the most stable.

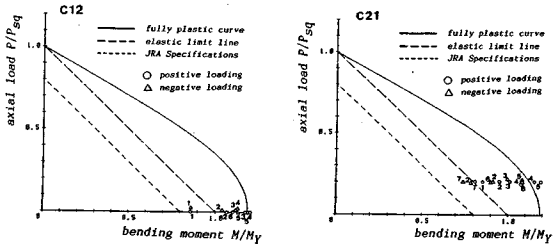

Fig. 10 Interaction Curves of Axial Thrust and Bending Moment. C-types.

Figs. 11 to 13 show the relationships between the bending moment and the curvature, both non-dimensionalized by the bending moment of the first yield, M_Y, and the corresponding curvature, Φ_Y. When the axial thrust is absent, the envelope curve of the peak moments on the $M-\Phi$ curves under repetitive bending seems to be an $M-\Phi$ curve under a simple non-repetitive bending.

On the other hand, in the case of the presence of the axial thrust, it is shown that the envelope curve of the peak moments can not be expected since the $M-\Phi$ curves gradually change depending on their histories of the elasto-plastic deformations.

Now, if the "ductility" is defined by ratio Φ/Φ_Y at the peak bending moment, then from these figures the following interesting remarks will be made on the ductility : (i) A-types : the ductility is a little above 2.0 when the axial thrust is absent and a little less than 1.5 when it is present, (ii) B-and C-types : the ductility is about 4.0 when the axial thrust is absent and a little less than 2.0 when it is present.

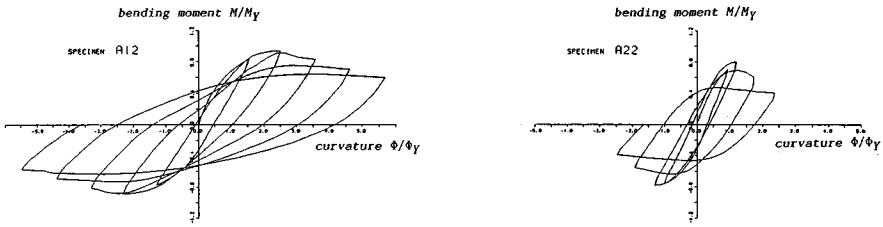

Fig. 11 Moment-Curvature Relationships. A-types.

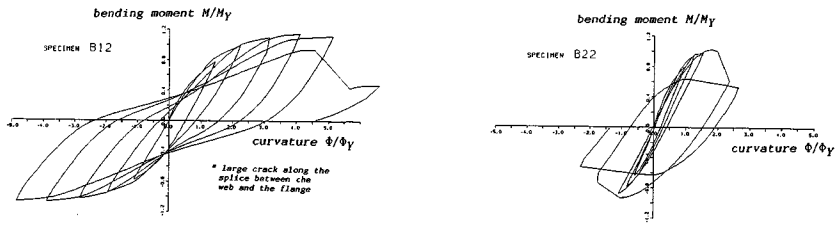

Fig. 12 Moment-Curvature Relationships. B-types.

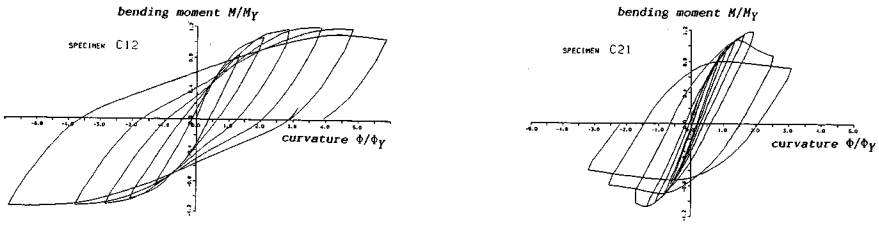

Fig. 13 Moment-Curvature Relationships. C-types.

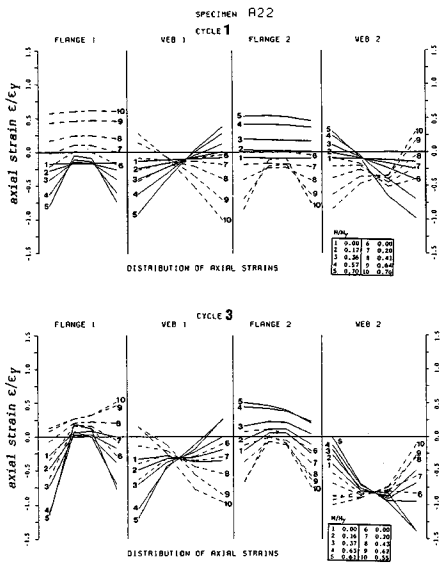

Fig. 14 Examples of Strain Distributions. Specimen A_{22}.

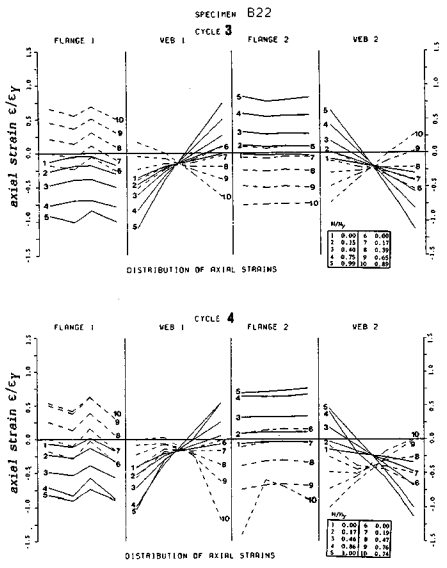

Fig. 15 Examples of Strain Distributions. Specimen B_{22}.

(2) In-Plane strain distributions and out-of-plane deflectional wave forms

Figs. 14 and 15 show a number of examples of the distribution of the in-plane axial strains, for A-type and B-type specimens, respectively. The flanges of the A-type show the typical postbuckling pockets ; whereas, those of B-type show rather uniform distribution.

Fig. 16 shows examples of the out-of-plane deflectional wave forms of Specimens A_{12}. The buckled wave forms become apparent as the number of cycles increases.

From the results of modal analysis for the out-of-plane deflections of the flanges, the A-type specimens are found to fail with 3.5 half waves and 1 half wave in the longitudinal and transverse direction, respectively. Also, the B- and C-type specimens are found to fail with 6 or more than 7 half waves in the longitudinal direction for the flange plate panels, but with 1 half wave in both the longitudinal and transverse directions for overall stiffened flanges.

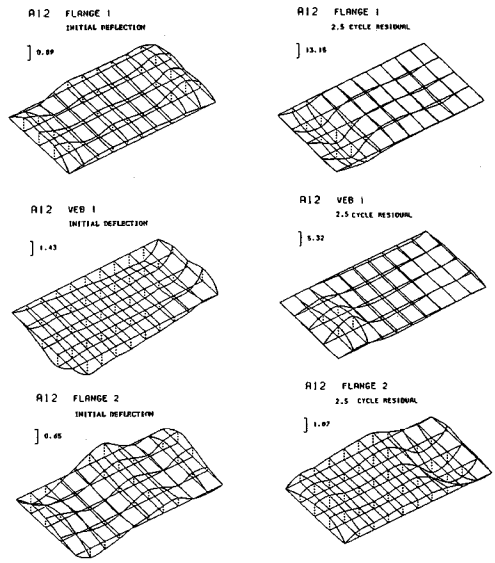

Fig. 16 Out-of-plane Deflectional Wave Forms. Specimen A_{12}.

As a result, it is found that the overall strength, M/M_Y, of box beam-column can be carried by the webs even after the flanges reach their peak bending moments, and then, the reduction of the bending moments which the webs can support decreases the overall strength of box beam-column. Here, the reduction of the web-moments is seen to be caused by the interactive deformations of the webs due to the elastic buckling of the flanges for the A-type specimens ; whereas it is mainly caused by the plastification of the webs for the B- and C-type specimens.

4. CONCLUSIONS AND ACKNOWLEDGMENTS

The following conclusions may be drawn from the study :

(1) The most influential parameters on the load-carrying capacity of steel box beam-columns would be the generalized width-thickness parameter, R, and the relative flexural stiffness, γ, of the stiffened plates. Depending on γ, the specimens are classified into A, B and C types. The failure of each type has occurred in the manner described in the following :

A-type The elastic buckling occurs in the compression flange. Then, the out-of-plane deflections grow significantly both in flanges and webs, and thus, the strength decreases. The ultimate strength lies within the elastic domain.

B-type The flange plates can almost reach the squash load. After the mature plastification of webs and the significant growth of the out-of-plane deflections, the ultimate strength decreases. The strength is found to be between the linear interaction of the initial yielding and the fully plastic interaction curve.

C-type The descriptions on B-type hold here too, except for the fact that the strength is found to be very close to the fully plastic interaction curve.

(2) The effect of the axial thrust corresponding to the load from the superstructure can be described in the following :

A-type It significantly reduces the maximum static strength, and the subsequent peak loads after the maximum static strength.

B- and C-types It does not significantly affect the maximum static strength ; but it significantly reduces the subsequent peak loads after the maximum static strength. When the axial thrust exists, the curvatures corresponding to the peak loads decrease. From this reason, the envelope curve of peak loads such as found in the case without the axial thrust can not be expected.

(3) The failure wave form of the flange plates are found as follows :

A-type 3.5 half waves in the longitudinal direction ; and 1 half wave in the transverse direction.

B- and C-types 6 or more than 7 half waves in the longitudinal direction.

(4) The curvature corresponding to the maximum load divided by the curvature of the first yield, namely Φ/Φ_Y is found as follows :

A-type A little above 2.0 when the axial thrust is absent ; a little less than 1.5 when it is present.

B- and C-types About 4.0 when the axial thrust is absent ; a little less than 2.0 when it is present.

The authors wish to express appreciation to President Yoshiji Niwa of Fukui National College of Technology and the Professor Emeritus of Kyoto University for his support and valuable suggestions.

This study was financially assisted by the Hanshin Express Highway Authority. The most of the computations were performed using M 382 of the Data Processing Center of Kyoto University.

REFERENCES

1) Kasai, K. and Egor P. Popov : Cyclic web buckling control for shear link beams, Journal of Structural Engineering, ASCE, Vol. 112, No. 3, pp. 505~523, 1986.

2) Hjelmstad, K. D. and Egor P. Popov : Cyclic behavior and design of link beams, Journal of Structural Engineering, ASCE, Vol. 109, No. 10, pp. 2387~2403, 1983.

3) Malley, O. J. and Egor P. Popov : Shear links eccentrically braced frames, Journal of Structural Engineering, ASCE, Vol. 110, No. 9, pp. 2275~2295, 1984.

4) Popov, Egor P. and Mahin, S. A. : Cyclic inelastic buckling of thin tubular columns, Proc. of ASCE, Vol. 105, No. ST 11, pp. 2261~2277, 1979.

5) Roeder, C. W. and Egor P. Popov : Eccentrically braced steel frames for earthquakes, Proc. of ASCE, Vol. 104, No. ST 3, pp. 391~412, 1978.

6) Popov, Egor P. and Petersson, H. : Cyclic metal plasticity : Experiments and theory, Proc. of ASCE, Vol. 104, No. EM 6, pp. 1371~1388, 1978.

7) Popov, Egor P. and Bertero, V. V. : Seismic analysis of some steel building frames, Proc. of ASCE, Vol. 106, No. EM 1,

pp. 75～92, 1979.

8) Fukumoto, Y. and Kusama, H. : Alternating buckling behavior of thin-walled steel box beams, Journal of Structural Engineering, JSCE, Vol. 31 A, pp. 37～50, 1985 (in Japanese).

9) Iwasaki, T. et al. : Perfectly alternating loading tests on steel pier models, Public Works Research Institute, Ministry of Construction, P. W. R. I Report, No. 2147, 1984.

10) Japan Road Association : Specifications for highway bridges with commentary, 1973 (in Japanese).

11) Nakai, H. et al. : A survey on steel rigid frame bridge piers, Bridge and Foundation Engineering, No. 6, pp. 43～49, 1982 (in Japanese).

12) Seeger, T., Hoffmann, M. und Klee, S. : Die Beurteilung der Bauteilschwingfestigkeit auf der Basis örtlicher Beanspruchungen, Kurt-Klöppel-Gedächtnis-Kolloquim, THD-Schriftenreihe Wissenschaft und Technik, S. 409～448, 1986.

13) Uetani, K. : Symmetry limit theory and steady-state limit theory for beam-columns subjected to alternating plastic bending, Doctoral Dissertation, Kyoto University, 1984.

14) Niwa, Y., Watanabe, E. and Isami, H. : Automated structural testing using microcomputer system, Proc. of JSCE, No. 332, pp. 145～158, 1983.

15) Niwa, Y., Watanabe, E. and Isami, H. : Automated testing of thin-walled steel structures under repetitive loading by microcomputer system, Proc. 2nd Int. Conf. Civil Eng. Comp., Vol. 2, pp. 337～343, 1985.

16) DIN 4114 Blatt 1, Stahlbau, Stabilitätsfälle (Knickung, Kippung, Beulung), Berechnungsgrundlagen, Richtlinien, 1953.

17) DIN 4114 Blatt 2, Stahlbau, Stabilitätsfälle (Knickung, Kippung, Beulung), Berechnungsgrundlagen, Richtlinien, 1953.

18) Japan Road Association : Specifications for highway bridges with commentary, 1980 (in Japanese).

(Received December 3 1986)